NANO LETTERS

pubs.acs.org/NanoLett Letter

# Resonant Laser Printing of Optical Metasurfaces

Xiaolong Zhu,* Jacob Engelberg, Sergei Remennik, Binbin Zhou, Jonas Nyvold Pedersen, Peter Uhd Jepsen, Uriel Levy,* and Anders Kristensen*

Cite This: https://doi.org/10.1021/acs.nanolett.1c04874 Read Online

ACCESS | Metrics & More | Article Recommendations | Supporting Information

**ABSTRACT:** One of the challenges for metasurface research is upscaling. The conventional methods for fabrication of metasurfaces, such as electron-beam or focused ion beam lithography, are not scalable. The use of ultraviolet steppers or nanoimprinting still requires large-size masks or stamps, which are costly and challenging in further handling. This work demonstrates a cost-effective and lithography-free method for printing optical metasurfaces. It is based on resonant absorption of laser light in an optical cavity formed by a multilayer structure of ultrathin metal and dielectric coatings. A nearly perfect light absorption is obtained via interferometric control of absorption and operating around a critical coupling condition. Controlled by the laser power, the surface undergoes a structural transition from random, semiperiodic, and periodic to amorphous patterns with nanoscale precision. The reliability, upscaling, and subwavelength resolution of this approach are demonstrated by realizing metasurfaces for structural colors, optical holograms, and diffractive optical elements.

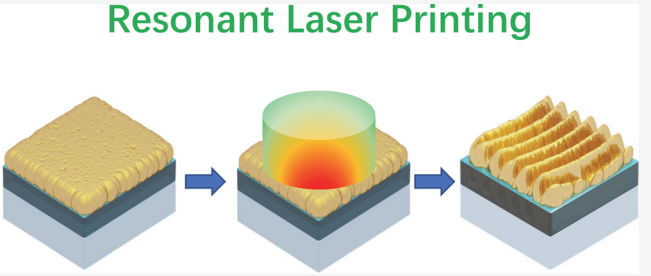


**KEYWORDS:** *Optical metasurface, Resonant laser printing, Optical cavity, Structural color, Holography*



## INTRODUCTION

Advances in nanophotonics and nanofabrication have enabled optical metasurfaces,[1] a new class of ultrathin optical elements comprising arrays of nanoscale artificial atoms which collectively control the amplitude, phase, polarization, and spectral properties of light. Control of light in the time, frequency, and space domains by ultrathin optical metasurfaces[2] has enabled a range of novel applications such as skin cloaks,[3] metalenses,[4] and quantum devices.[5] However, the structural complexity of optical metasurfaces poses a challenge to their upscaling and large-volume applications. This calls for new routes of fabrication at the nanoscale. Ultrafast laser pulses can create and manipulate states of matter in the mechanical,[6] chemical,[7] electric,[8] and magnetic[9] domains. They can also be used to redefine and reconfigure metasurfaces.[10]

Laser processing, which usually relies on strong interactions between light and matter, is already widely implemented in industrial manufacturing for photonic devices.[11−13] Conventional laser processing technologies rely on the high energy density in a focused beam derived from a pulsed laser,[14] in combination with ultrashort pulses (femto- to picoseconds) to spatially confine the laser-induced heating.[15,16] For instance, ultrafast femtosecond lasers are recently introduced for postprocessing as-prepared metasurfaces,[17] where the near-infrared femtosecond pulses are typically not in resonance with resonant features of the plasmonic or dielectric nanoantennas resonating at the visible. In contrast, resonant laser printing (RLP), applied in the current work, utilizes resonant features with enhanced light confinement in plasmonics[18] or high-index-material resonators.[19] In the absence of coupling between individual resonators, the random spatial position of these will not affect the spectral response of the ensemble. However, for optical systems with collective architectures of tightly coupled resonators, many-body interactions might offer unique adaptability and could possess novel functionalities through emerging transient or persistent structures. By employing RLP within an optical cavity with near-perfect light absorption, we successfully print the stabilized ordered states for use as functional optical metasurfaces.

## RESULTS

**Resonant Laser Printing within an Optical Cavity.** Coherent light processing of an ensemble of coupled optical resonators may lead to their dissipative self-organization through collective interactions.[20−22] Here, we propose an optical system that is driven by a pulsed laser emitting at a resonance frequency of the system, leading to self-organized surface structures with self-adaptive morphology through a phase modulation feedback; see Figure 1a. An optical cavity, Figure 1b,c, comprising an ultrathin film on lossless dielectric

Received: December 18, 2021
Revised: March 12, 2022

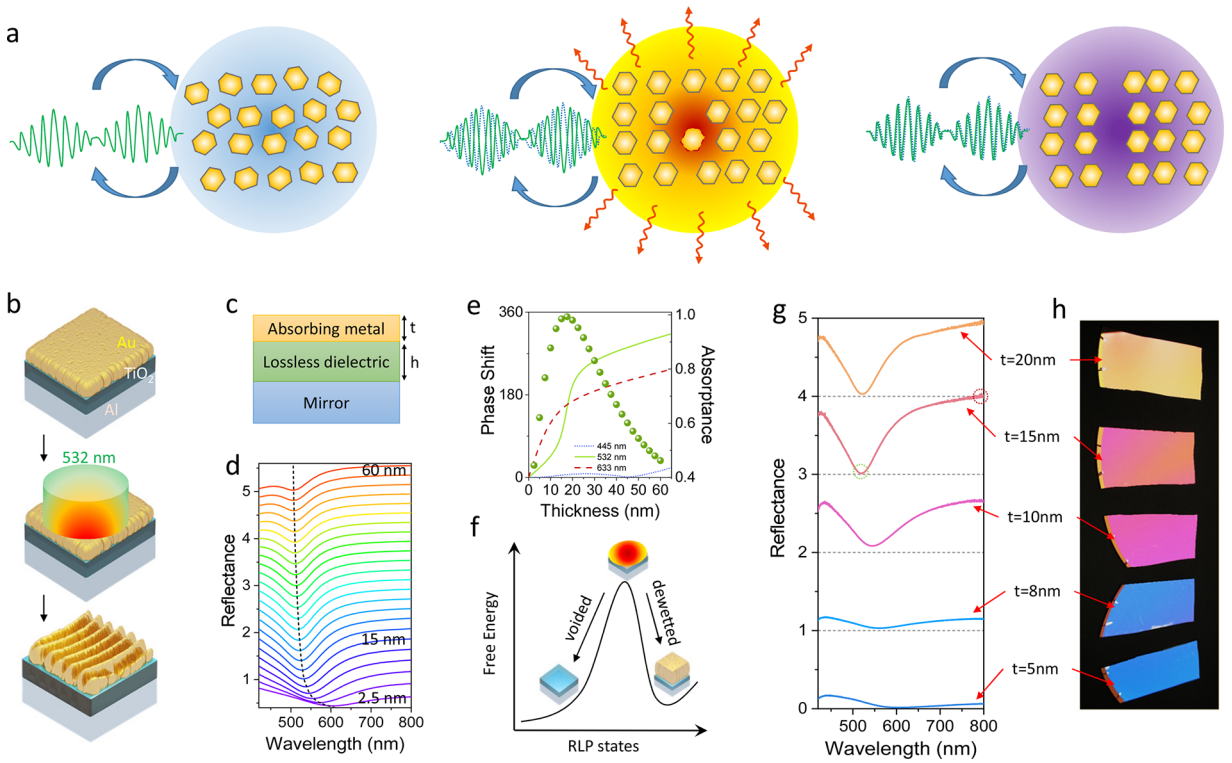


**Figure 1.** (a) (Left) Coherent light interacts with an ensemble of randomly distributed resonators in an optical cavity. (Middle) The drive light intensity just at the threshold can heat up the system and thus shift it to be off the critical condition. In the presence of dissipation, novel orders of crystalline and structure can be created in a radiative cooling process where the spontaneously emitted energy introduces pronounced entropy. (Right) The cooled system after a single laser pulse treatment presents a reflective state with constructive interference for the input light. (b) Schematics of the FP-type hybrid metasurface with Au-$TiO_2$-Al coatings. The polarized in-resonance laser pulses interact strongly with the optical cavity, making the metasurface extremely absorbing across the illuminated area, which creates ripples and modifies the optical cavity to an off-resonance state. (c) Schematic of the hybrid metasurface indicated with parameters. (d) Simulated reflectance spectra for structures with different thickness $t$ of gold atop $h$ = 51 nm $TiO_2$. The spectra are stacked with a +0.2 offset. (e) Lines: Simulated phase shift between the gold film and the $TiO_2$/Al substrate as a function of the film thickness at different wavelengths. Dots: Corresponding values of absorptance at 532 nm, extracted as 1-$R$ from reflectance data ($R$) in panel d. (f) This critical position is an unstable equilibrium: a small perturbation will cause it to fall to one of the two states, voided or dewetted, and both can decrease the energy absorption and shift the optical phase. The final state is not symmetric and unpredictable. (g) Measured reflection spectra with different thicknesses of gold. The spectra are stacked with a +1.0 offset. The circles indicate the measured reflection minimum of 1% and reflection maximum of (over) 99% for the case of $t$ = 15 nm. (h) Variety of color appearances formed by coating gold with nanometer thicknesses.

($TiO_2$), is embedded between a perfect conductor (Al) and a thin, semitransparent, lossy metal film (Au). The system is designed to support attenuated Fabry−Perot-type interference,[23] with a critical coupling condition, observed as a reflectance minimum. Initially, the drive laser is in resonance with this reflectance minimum, and the driving laser pulse reduces the crystalline fluctuations of the ensemble of Au grains introduced in electron-beam deposition (Figure 1a). Resonant absorption of light heats the ensemble to a temperature just at the threshold for a phase change or reflow of the Au in the presence of energy dissipation. Immediately hereafter, the critical coupling condition is detuned from the drive laser frequency. Even a slight change in resonance frequency will reduce absorption of laser light, hindering further energy accumulation and thereby suppressing the energy consumption in the dissipative system. This system enables the formation of stable ordered structures. Here, we use ordered photons (coherent light) to create structural order via radiative energy dissipation. As shown in Figure 1b, laser light is resonantly absorbed in the top metal layer and drives a dewetting process of this layer. Subsequently self-organized patterns are formed in order to dissipate the energy. Laser-induced periodical surface structures (LIPSS)[24,25] can be generated via the constructive interference pattern in the surface as sketched.

In fabrication, an ultrathin amorphous $TiO_2$ film is deposited by atomic layer deposition (ALD) on top of an optically thick Al film to approach the limit of no penetration of light into the metal and no absorption in the visible regime.[26] It should provide a reflective phase shift $\Delta\phi = -2kh\cos\theta + \pi$, where $k$ is the wavenumber, $h$ is the thickness of the dielectric, and $\theta$ is the angle of incidence. One special case with $h \simeq \lambda/4n$ supports the resonant condition at normal incidence where a round trip accumulates a $2\pi$ phase shift. For working exactly at the laser frequency of 532 nm, we used a $TiO_2$ thickness $h$ = 51 nm. Deposition of a thin lossy metal film on top of the resonant cavity mimics adding damping to an oscillator (Figure 1b), which modifies the amplitude of the reflection spectrum.[27] Simulated reflection spectra for structures with gold films of thickness $t$ between 2.5 and 60 nm atop $h$ = 51 nm thick $TiO_2$ are shown in Figure 1d. As the thin gold film is semi-transparent (and partly reflecting), the amplitude of the interference increases with film thickness $t$ up to ~15 nm and decreases for thicker films. The resonant frequency blue shifts


https://doi.org/10.1021/acs.nanolett.1c04874
Nano Lett. XXXX, XXX, XXX−XXX

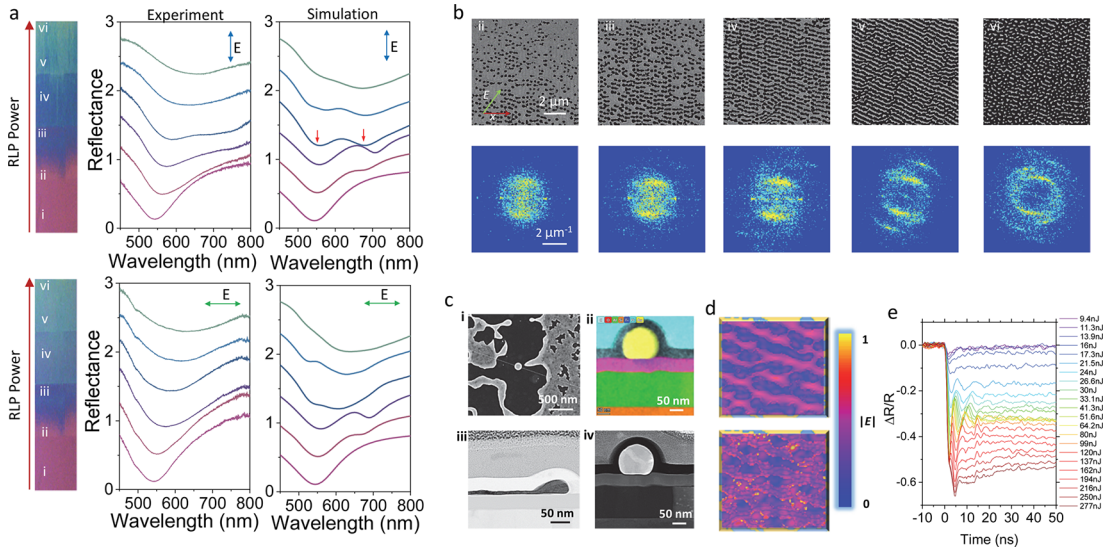


**Figure 2.** (a) (Left) Photographs of laser printed areas. With linearly increased laser intensities, the laser treated surfaces undergo a structural color change from magenta, blue, to cyan. (Middle) Measured reflection spectra under white light illumination with different polarizations. (Right) Simulated reflection spectra under white light illumination with different polarizations. The spectra are stacked with a +0.4 offset. (b) (Top) SEM images of laser printed surfaces, corresponding to the labeled areas (ii–vi) in (a). The writing direction in the *x*-axis of the laser beam and the polarization of the laser beam used for writing for all of the images (ii–vi) are indicated in image (ii). (Bottom) Corresponding fast Fourier transform patterns. (c) (i) SEM image showing the region which was exposed (left) and not exposed (right) to laser. The dashed line denotes the FIB cut that was performed later. It is already possible to see that grains are larger in regions exposed to the laser. (ii) STEM EDS Map of a cut along the dashed line in (i). It is focused on the region in the middle of the FIB cut. Silicon, Al, and $TiO_2$ (combination of blue Ti and red oxygen generates pink color) are labeled with different colors, respectively. (iii) and (iv) Cross-section STEM images indicating the right part (iii) and the sphere (iv) of the cut. (d) Simulated light field distributions for the guided (the left panel) and plasmonic (the right panel) modes at around 558 and 676 nm (as labeled in a), respectively. (e) Time traces of the changed reflectance for the case of Au thickness $t$ = 10 nm and driven at different energy values.

with increasing thickness, attributed to the further accumulated phase shift relative to the internal reflections.

In order to describe the critical coupling condition in our system, we calculated the phase shift between the gold film and the bare $TiO_2$ Fabry–Perot (FP) cavity as a function of top Au film thickness $t$, and for three different wavelengths: 445, 532, and 633 nm. With a suitable choice of $t$, a critical coupling condition at the resonant frequency (532 nm) can be achieved with a $\pi$ phase shift. At wavelengths of 532 and 633 nm, the phase shift increases with increasing Au film thickness $t$. The phase modulation of the reflected light beam from the resonant cavity can be largely enhanced at a resonance frequency of 532 nm. For shorter and longer wavelengths (e.g., 445 and 633 nm), the electromagnetic fields in the resonant cavity will be suppressed in the dielectric layer or be evanescent to the air, leading to weaker interactions within the gold layer. At critical coupling, the absorptivity of the structure reaches unity at the resonant frequency where the impedance changes more quickly, and the slope of the phase change is also the maximum, as shown in Figure 1e (see also the Supporting Information, Figure S1).

The designed structure with the critical coupling condition is an out-of-equilibrium system upon laser illumination. At sufficient laser power, the system undergoes a structural phase transition into a quasistable, self-organized state where the thin metal film accumulates to thicker elements in order to dissipate the energy through a thermodynamic process. The dewetting-induced aggregation of the metal leads to changes in the optical path length and optical phase distributions away from the critical coupling condition. For a driving laser pulse just at the threshold, the perturbation of the film thickness due to small fluctuations in metal reflow along the transverse interference directions will give feedback into an optical phase perturbation because of the variation in the optical path lengths. As the energy absorptivity is already optimal for the metal film with the critical thickness, these optical phase perturbations will further reduce the energy absorption and thus provide a feedback loop of optical phase modulation. The mechanism that regulates energy dissipation in such a system is illustrated in Figure 1f, where in-resonance coherent wave excitation naturally leads to energy-dependent structural self-organization with feedback (Supporting Information, Figure S2).

To test our hypothesis, we fabricated a series of FP cavity samples with different thicknesses of the top Au film. Figure 1g shows the measured reflection spectra of samples with Au films of thickness $t$ from 5 to 20 nm. As expected, the optical metafilm stack can act as a perfect absorber at a narrow band for $t \approx 15$ nm. This is the simplest realization of a single-channel coherent perfect absorber—a time-reversed counterpart to laser emission—where incident coherent optical fields are perfectly absorbed within a resonator that contains a loss medium instead of a gain medium.[28] As mentioned above, the thin metallic films have granular or percolation structures (see Supplementary Figure S2). The energy loss to the conduction electrons in these structures increases dramatically because of additional boundary effects, leading to measured low reflections for $t < 10$ nm, as shown in Figure 1g. Figure 1h shows photographs of the corresponding samples, creating a spectrum of colors including blue, pink, and yellow for different $t$ values. Under appropriate conditions, interference can persist in ultrathin, highly absorbing films of a few to tens


https://doi.org/10.1021/acs.nanolett.1c04874
Nano Lett. XXXX, XXX, XXX–XXX

of nanometers in thickness.[29] This design presents a simple and low-cost structural color generation method based on thin-film interference, which does not rely on any advanced nanoscale lithography, and is easy to scale up.

**Resonant Laser Printing (RLP) of Surface Structures.** RLP on such thin-film optical resonators is a flexible postprocessing technology for mass customization of optical devices. In the RLP process, rapid melting allows for surface-energy-driven collective morphology changes with associated modification of the optical properties of the reflected or scattered light from the surface. By controlling the RLP process, the material and structural properties of the optical devices can be manipulated with high precision.

We first investigate the influence of the RLP power by printing a bitmap stripe on the sample with a Au film thickness $t$ = 10 nm, applying single pulse laser energies from 0 to 1.9 nJ, which are spatially distributed with a linear gradient. Here, a micron-sized laser focus spot (1−2 $\mu$m) and a subdiffraction-limited step size of 250 nm enabled laser writing features and gradients at the nanoscale. It thus allows subwavelength supercell pixels which can provide a spatial resolution exceeding 100 000 DPI. This relies on a Gaussian distribution of the laser energy, where only a small central region overcomes the threshold for laser modification. The lithography-free laser processing method without any comprehensive and costly developing or etching processes makes the upscaling of the metasurfaces more feasible. Stitching errors are observed between scanning domains (50 × 50 $\mu m^2$) of the combined piezo and motorized stages that were used in the experiment. As shown in Figure 2a (left column), the printed color varies from pink to cyan in the photos taken under different polarizations.

Next, we show that the printed structures result in different color hues when illuminated with visible light of different polarizations. This indicates that the rotational symmetry is lifted by the RLP—colors can be switched through polarization tuning. The middle and right columns in Figure 2a show the measured and simulated spectral data corresponding to each color positions as presented in the left photos. The spectra measured under perpendicular polarized incident light display double resonant dips for positions iii and iv, which are different from the spectra measured under the other polarization.

Representations of self-organized nanostructures produced by RLP are summarized in Figure 2b. It should be mentioned that the writing laser beam is polarized at an angle of 45° ($E$) relative to the direction of beam translation ($x$), as indicated in image (ii). Note that the orientation of the stripes in the images (iv) and (v) is perpendicular to the polarization of the laser beam used for writing.

We further characterized the structures with processing doses of 0.38, 0.75, 1.1, 1.5, and 1.9 nJ by Fourier transformation of the scanning electron microscope (SEM) images. These results show that RLP on thin-film optical resonators can provide structures—from disordered, semi-periodic, periodic, to amorphous.

When the thin gold film is exposed to a laser drive just at the threshold of initializing the film change, the absorption of the energy by nanoscale gold clusters leads to local increase in temperature. Heated elements self-organize spontaneously. Figure 2c shows a RLP-treated region. It is observed that the grains become larger in the exposed region with a typical size of about 30−70 nm. It is also seen that the exposed region is converted to a "droplet" shape, in order to reduce the surface energy, and TEM imaging indicates that material in the droplet is crystallized.

At high laser power, the boundary "defects" will separate into gaps and stripes following the interference pattern of the coherent light source and be fixed as a periodic structure. By further increasing of the laser power, the large energy input drags the system far from the critical condition, giving rise to extra randomness in the system. The competition between the randomness and the polarization is clearly indicated in the Fourier transformation images (Figure 2b), leading to the collective structural evolution with controllable randomness or periodicity. Numerical simulations in Figure 2d further show that the spectral responses can be dynamically tuned by changing the surface morphology, while both the guided (the left panel) and plasmonic (the right panel) modes can be excited as depletion bands in the simulated reflection spectra in $y$-polarization shown in Figure 2a (labeled by arrows).

We apply a time-resolved in situ optical pump−probe technique to probe the dynamic changes of the reflectance of the system in order to quantify the kinetics of the Au thin films. Figure 2e shows time-resolved reflectance of Al-$TiO_2$-Au thin-film resonators (Au film thickness $t$ = 10 nm) irradiated with single in-resonance (wavelength 532 nm) laser pulses of different pulse energies. Laser-induced self-organization dynamics is a fundamental process of matter that is complex at the microscopic level.[30] Once we pump a region of the nanoplasmonic heterostructure (Au nano clusters atop the FP cavity) with an in-resonance Gaussian incident beam, we can consider them as a many-body system made of an ensemble of coupled optical nano-oscillators, similar to the prototype model of coupled mechanical oscillators. Once a pump field deposits energy in a finite region in the core of the heterostructure, the coherence-driven complex nanosystem in an optical cavity undergoes a state where the modes initially oscillate out of phase but eventually synchronize owing to the nonlinear coupling between neighboring Au nanoclusters. The time-resolved plot of dynamics (Figure 2e) displays large oscillations in reflectance. It is important to note that these damped oscillations are observed directly after the laser pulse. This result indicates that the self-organization, typically realized in the physics of nonequilibrium processes, plays an important role in our system. It should be mentioned that the optical cavity with a critical condition makes the resulting organization of gold clusters robust and able to self-feedback on substantial perturbations (see also Supporting Information, Figure S3).

**Resonant Laser Printing of Structural Colors.** Nature provides numerous examples of bright coloration from self-organized photonic crystals.[29] Structural color based on individual resonators, such as plasmonic and dielectric nanoantennas, allows for color printing with subdiffraction resolution.[31−34] As an alternative method to liquid crystal enabled tuning of plasmonic metasurfaces,[35,36] laser printing is a cost-effective postprocessing technique that can tune the plasmonic colors of nanostructure arrays produced by nanofabrication techniques.[18,37,38] In contrast, the RLP induced self-organized metasurfaces presented here offer subwavelength resolution without lithography, and it is easy to upscale for large-volume production. To demonstrate the printing resolution of a self-organized structure that can be laser-induced, we pattern an image using the same micron-sized laser focus spot (2−4 $\mu$m) and a subdiffraction-limited


https://doi.org/10.1021/acs.nanolett.1c04874
Nano Lett. XXXX, XXX, XXX−XXX

step size (250 nm) but digitally varied doses according to the gray-scale depth of the image.

Self-assembly, or more specifically directed self-assembly, such as in block copolymer methods can provide a high-resolution pattern, where the resolution is limited by the molecular scale (5−50 nm).[39] Here, we use a subdiffraction-limited step size of 250 nm and a focus spot size of about 2−4 $\mu$m to laser print 100−200 nm-sized gold clusters. The clear color contrast demonstrates the feasibility of such ultrathin self-organized metafilms. We then verify the graphically pixelated pattern by an SEM image and highlight the correlation between structural colors and the morphology of self-organized film shown in Figure 3a. By arranging these

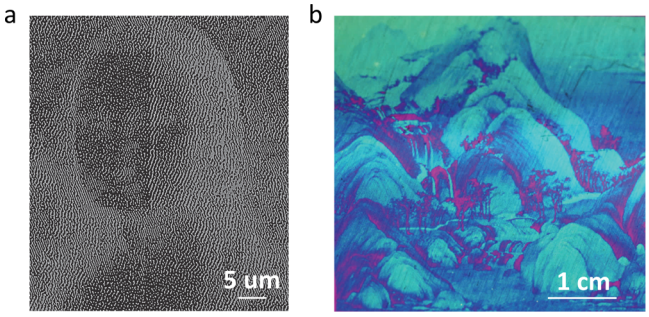


**Figure 3.** (a) SEM image of the laser-induced structural pattern, which shows self-organized features with a subwavelength scale. (b) Photograph of a structural color pattern which is printed on the sample with a gold film thickness of 15 nm. Photography credit: *A Thousand Li of Rivers and Mountains* (part), created by Wang Ximeng in the Northern Song Dynasty (960−1127), with the permission from the Palace Museum.

coded RLP bits (in eight-bit depth) with predesigned coding sequences from the image data map on our flat surface, a variety of self-organized structures of the coded metasurface retrieve the color pixel information from the reflection responses of the semirandom surface. A high resolution with particle sizes down to 100 nm and subwavelength patch sizes is observed.

The 2D disordered metasurface provides the optical "randomness: with broadband and wide-angle properties,[40] which exhibits additional unique features for structural color generation such as a wide angular scattering range, excellent stability, and a noniridescent color appearance with a high saturation. To demonstrate the color-rendering capability, an image is also drawn on metafilm stacks with a gold film of 15 nm. The resulting optical images are shown in Figure 3b; see also the reflectance spectra measurements in the Supporting Information, Figure S4. Although we used a large laser spot (15−20 $\mu$m) to implement the centimeter-scale structural color printing, the resulting self-organized surface structures show a biomimicry mesh-like architecture which possesses features still down to 100 nm, as shown in Supporting Information, Figure S5.

**Resonant Laser Printing of Holograms.** Holography is the most promising approach to fully tailor the wavefronts of light, but the typical large pixel size, complex realization, and costly device impose limitations in high-performance applications such as 3D image projection and big data storage. To obtain a pronounced phase shift modulation, the thickness of hologram samples has generally been above the optical wavelength scale, which hinders their compact integration. Metasurfaces provide novel solutions for achieving holograms within an ultrathin membrane, while nanoscale optical resonators implemented in the interface provide both phase and amplitude manipulation of the wavefront with an unprecedented spatial resolution.[41−43]

The creation of self-organized nanostructures in our system leads to not only amplitude modification but also optical phase modulation (Figure 4a and Supporting Information, Figure

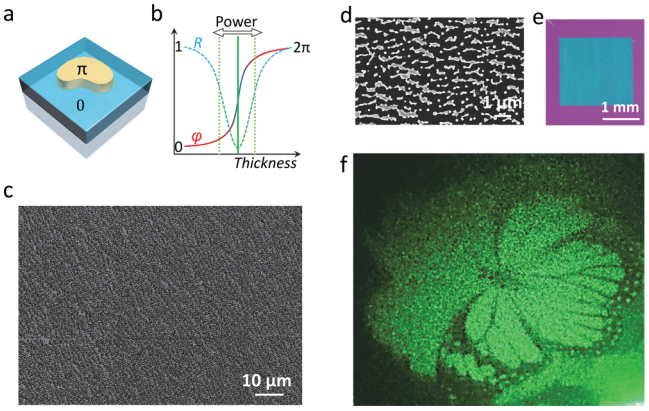


**Figure 4.** (a) Schematic of dewetting induced optical phase separation. (b) Schematic of laser printing power manipulated film thickness and amplitude/phase separation started from the critical point. (c) SEM image of a laser printed hologram. (d) SEM image of a detailed area. (e) Photo of a 532 nm laser printed hologram. The greenish appearance reflects the high reflection at the printing wavelength. (f) Laser printed hologram of a butterfly (photography credit: Xiaolong Zhu/Jesper Scheel).

S6). With a sufficient drive power applied to a sample at the critical condition (perfectly absorbing), a coexistence system of two steady states, voided and dewetted, can be printed, as shown in Figure 4a. Typically, the optical phase difference in between the two states is proportional to the applied power, while the off-resonance condition leads to a printed film which is highly reflective (over 50%) at the critical printing frequency, as shown in Figure 4b. Our technique further allows us to generate high-quality holograms, which are large area and high density, containing printed supercell pixels with a diffraction-limited size of 500 nm, as shown in Figure 4c,d. As in the previous color printing designs, the laser-induced supercell library (or laser power map) is employed to optimize the design to get library elements covering all phases needed for the desired hologram. We performed a set of experiments to prove the concept. First, we used a fast Fourier transform method to convert gray-scale images into phase patterns in four-bit gray levels with 4K by 4K (16M) pixels, leading to laser printed areas of 2 mm-by-2 mm, as shown in Figure 4e. Note that the phase shift increases when the laser printing power of the thin film increases. For instance, by simply ablating material from the surface, we can create a $\pi$ phase shift; see the discussions in the Supporting Information, Figure S6.

By laser printing, we generated the holographic images through the reconstruction of wavefronts of light with the calculated amplitude and phase information. By the shining of a laser beam on the printed metasurfaces, the holographic images are diffracted with a small projection angle of about 10°. The reconstructed image was displayed on a white screen and recorded with a digital camera. Figure 4f shows the


https://doi.org/10.1021/acs.nanolett.1c04874
Nano Lett. XXXX, XXX, XXX−XXX

holographic image at 532 nm illumination. The proposed technique using nanosecond single pulsed laser printing makes it possible to reconstruct high-quality and bright 3D images without costly and complicated nanofabrication. Our high-definition holograms fabricated as reflective metasurfaces yield high-contrast images with a measured diffraction efficiency of about 11% at a wavelength of 532 nm. (See also the optical diffraction elements in Supporting Information, Figure S7.) By introducing the interfacial phase shifts, our approach with free-form, self-organized nanostructures enables the realization of metasurface holograms and flat optical elements with unprecedented capabilities. Hologram movies may come to the real world and be completely re-envisioned with our solution, by replacing expensive, time-consuming, and sophisticated electron-beam nanolithography procedures.[44] Furthermore, metasurface-driven displays can be further improved through RLP nanopatterned color metasurface mirrors.[45]

## CONCLUSION

In conclusion, our experiments demonstrate self-organized optical metasurfaces realized by coherent light postprocessing, enabling applications in structural color printing, optical holograms, and diffractive optical elements. Efficient control realized by in-resonance collective manipulation at the critical condition permits reliable switching of optical amplitude and phase levels with an ultrafast transient response, while the self-phase modulation gives feedback and stabilizes the desired structures at the nanoscale. The developed principles of coherent light postprocessing, in combination with the recent development of nanophotonics, may pave the way for the creation of unprecedented photonic devices.

## ASSOCIATED CONTENT

### Supporting Information

The Supporting Information is available free of charge at https://pubs.acs.org/doi/10.1021/acs.nanolett.1c04874.

Detailed experimental part of thin-film deposition, numerical simulation, laser printing systems, optical setups, STEM sample preparation, and time-resolved transient measurement. Supplementary Figures S1−S7 of a phase shift diagram, randomness in the deposited film and scattering model, time-resolved transient response at the critical point, reflection spectra of laser printed samples with different thicknesses, photo and SEM images of large-scale laser printing samples, simulated phase shifting, and demo of diffractive optical elements (PDF)

## AUTHOR INFORMATION


### Corresponding Authors

**Xiaolong Zhu** − *State Key Laboratory of Precision Spectroscopy, School of Physics and Electronic Science, East China Normal University, Shanghai 200241, China; Department of Health Technology, Technical University of Denmark, Kongens Lyngby 2800, Denmark;* orcid.org/0000-0003-4670-7901; Email: xlzhu@lps.ecnu.edu.cn

**Uriel Levy** − *Department of Applied Physics, The Faculty of Science, The Center for Nanoscience and Nanotechnology, The Hebrew University of Jerusalem, Jerusalem 91904, Israel;* orcid.org/0000-0002-5918-1876; Email: ulevy@mail.huji.ac.il

**Anders Kristensen** − *Department of Health Technology, Technical University of Denmark, Kongens Lyngby 2800, Denmark*; Email: akri@dtu.dk

### Authors

**Jacob Engelberg** − *Department of Applied Physics, The Faculty of Science, The Center for Nanoscience and Nanotechnology, The Hebrew University of Jerusalem, Jerusalem 91904, Israel;* orcid.org/0000-0002-7421-914X

**Sergei Remennik** − *Department of Applied Physics, The Faculty of Science, The Center for Nanoscience and Nanotechnology, The Hebrew University of Jerusalem, Jerusalem 91904, Israel*

**Binbin Zhou** − *Department of Photonics Engineering, Technical University of Denmark, Kongens Lyngby 2800, Denmark*

**Jonas Nyvold Pedersen** − *Department of Health Technology, Technical University of Denmark, Kongens Lyngby 2800, Denmark;* orcid.org/0000-0001-7642-8212

**Peter Uhd Jepsen** − *Department of Photonics Engineering, Technical University of Denmark, Kongens Lyngby 2800, Denmark;* orcid.org/0000-0003-3915-1167

Complete contact information is available at: https://pubs.acs.org/10.1021/acs.nanolett.1c04874


### Author Contributions

X.Z. and A.K. conceived the ideas. X.Z. fabricated the samples and performed the experiments. J.E. measured the phase shift. S.R. performed STEM imaging. B.Z. helped with the time-resolved measurement. A.K., U.L., J.N.P., and P.U.J. provided feedback on the experiments. All authors contributed to the writing of the manuscript.


### Funding

This work is supported by the Villum Fond through the Villum Experiment Project (No. 17400) and The Science and Technology Commission of Shanghai Municipality (No. 21DZ1101500). X.Z. also acknowledges the support from the Fundamental Research Funds for the Central Universities, the Overseas Expertise Introduction Project for Discipline Innovation (the 111 Project, Code B12024), the Zijiang Excellent Young Scholar, and the National Oversea High-level Youth Talent Plan.


### Notes

The authors declare no competing financial interest.

## REFERENCES


(1) Kildishev, A. V.; Boltasseva, A.; Shalaev, V. M. Planar Photonics with Metasurfaces. *Science* **2013**, *339*, 1232009.

(2) Yu, N.; Capasso, F. Flat optics with designer metasurfaces. *Nat. Mater.* **2014**, *13*, 139−150.

(3) Ni, X.; Wong, Z. J.; Mrejen, M.; Wang, Y.; Zhang, X. An ultrathin invisibility skin cloak for visible light. *Science* **2015**, *349*, 1310−1314.

(4) Khorasaninejad, M.; Chen, W. T.; Devlin, R. C.; Oh, J.; Zhu, A. Y.; Capasso, F. Metalenses at visible wavelengths: Diffraction-limited focusing and subwavelength resolution imaging. *Science* **2016**, *352*, 1190−1194.

(5) Wang, K.; Titchener, J. G.; Kruk, S. S.; Xu, L.; Chung, H.-P.; Parry, M.; Kravchenko, I. I.; Chen, Y.-H.; Solntsev, A. S.; Kivshar, Y. S.; Neshev, D. N.; Sukhorukov, A. A. Quantum metasurface for multiphoton interference and state reconstruction. *Science* **2018**, *361*, 1104−1108.

(6) Brooks, D. W. C.; Botter, T.; Schreppler, S.; Purdy, T. P.; Brahms, N.; Stamper-Kurn, D. M. Non-classical light generated by quantum-noise-driven cavity optomechanics. *Nature* **2012**, *488*, 476−480.
(7) Brumer, P.; Shapiro, M. Control of unimolecular reactions using coherent light. *Chem. Phys. Lett.* **1986**, *126*, 541−546.
(8) Paul, K.; Sengupta, P.; Ark, E. D.; Tu, H.; Zhao, Y.; Boppart, S. Coherent control of an opsin in living brain tissue. *Nat. Phys.* **2017**, *13*, 1111−1116.
(9) Kimel, A. V.; Kirilyuk, A.; Tsvetkov, A.; Pisarev, R. V.; Rasing, T. Laser-induced ultrafast spin reorientation in the antiferromagnet TmFeO3. *Nature* **2004**, *429*, 850−853.
(10) Wang, Q.; Rogers, E. T. F.; Gholipour, B.; Wang, C.-M.; Yuan, G.; Teng, J.; Zheludev, N. I. Optically reconfigurable metasurfaces and photonic devices based on phase change materials. *Nat. Photonics* **2016**, *10*, 60−65.
(11) Sugioka, K.; Cheng, Y. Ultrafast lasers-reliable tools for advanced materials processing. *Light: Science & Amp; Applications* **2014**, *3*, e149.
(12) Wang, Z.; Fang, Z.; Liu, Z.; Chu, W.; Zhou, Y.; Zhang, J.; Wu, R.; Wang, M.; Lu, T.; Cheng, Y. On-chip tunable microdisk laser fabricated on Er3+-doped lithium niobate on insulator. *Opt. Lett.* **2021**, *46*, 380−383.
(13) Hu, D.; Li, H.; Zhu, Y.; Lei, Y.; Han, J.; Xian, S.; Zheng, J.; Guan, B.-O.; Cao, Y.; Bi, L.; Li, X. Ultra-sensitive nanometric flat laser prints for binocular stereoscopic image. *Nat. Commun.* **2021**, *12*, 1154.
(14) Roberts, A. S.; Novikov, S. M.; Yang, Y.; Chen, Y.; Boroviks, S.; Beermann, J.; Mortensen, N. A.; Bozhevolnyi, S. I. Laser Writing of Bright Colors on Near-Percolation Plasmonic Reflector Arrays. *ACS Nano* **2019**, *13*, 71−77.
(15) Bonse, J.; Hohm, S.; Kirner, S. V.; Rosenfeld, A.; Kruger, J. Laser-Induced Periodic Surface Structures-A Scientific Evergreen. *IEEE Journal of Selected Topics in Quantum Electronics* **2017**, *23*, 109−123.
(16) Matthias, E.; Reichling, M.; Siegel, J.; Kading, O.; Petzoldt, S.; Skurk, H.; Bizenberger, P.; Neske, E. The Influence of Thermal-diffusion on Laser-ablation of Metal-films. *Applied Physics A-Materials Science and Processing* **1994**, *58*, 129−136.
(17) Lu, Y.; Hu, D.; Zhang, M.; Yang, L.; Li, J.; Cao, Y.; Li, X. Laser printing based on curvature-driven shape transition of aluminum nanodiscs. *Chin. Opt. Lett.* **2021**, *19*, 053602.
(18) Zhu, X.; Vannahme, C.; Højlund-Nielsen, E.; Mortensen, N. A.; Kristensen, A. Plasmonic colour laser printing. *Nat. Nanotechnol.* **2016**, *11*, 325−329.
(19) Zhu, X.; Yan, W.; Levy, U.; Mortensen, N. A.; Kristensen, A. Resonant laser printing of structural colors on high-index dielectric metasurfaces. *Science Advances* **2017**, *3*, e1602487.
(20) Fialkowski, M.; Bishop, K. J. M.; Klajn, R.; Smoukov, S. K.; Campbell, C. J.; Grzybowski, B. A. Principles and Implementations of Dissipative (Dynamic) Self-Assembly. *J. Phys. Chem. B* **2006**, *110*, 2482−2496.
(21) Bachelard, N.; Ropp, C.; Dubois, M.; Zhao, R.; Wang, Y.; Zhang, X. Emergence of an enslaved phononic bandgap in a non-equilibrium pseudo-crystal. *Nat. Mater.* **2017**, *16*, 808−813.
(22) Ropp, C.; Bachelard, N.; Barth, D.; Wang, Y.; Zhang, X. Dissipative self-organization in optical space. *Nat. Photonics* **2018**, *12*, 739−743.
(23) Kats, M. A.; Blanchard, R.; Genevet, P.; Capasso, F. Nanometre optical coatings based on strong interference effects in highly absorbing media. *Nat. Mater.* **2013**, *12*, 20−24.
(24) van Driel, H. M.; Sipe, J. E.; Young, J. F. Laser-Induced Periodic Surface Structure on Solids: A Universal Phenomenon. *Phys. Rev. Lett.* **1982**, *49*, 1955−1958.
(25) Huang, M.; Zhao, F.; Cheng, Y.; Xu, N.; Xu, Z. Origin of Laser-Induced Near-Subwavelength Ripples: Interference between Surface Plasmons and Incident Laser. *ACS Nano* **2009**, *3*, 4062−4070.
(26) Liu, N.; Mesch, M.; Weiss, T.; Hentschel, M.; Giessen, H. Infrared Perfect Absorber and Its Application As Plasmonic Sensor. *Nano Lett.* **2010**, *10*, 2342−2348.
(27) Hao, J.; Wang, J.; Liu, X.; Padilla, W. J.; Zhou, L.; Qiu, M. High performance optical absorber based on a plasmonic metamaterial. *Appl. Phys. Lett.* **2010**, *96*, 251104.
(28) Wan, W.; Chong, Y.; Ge, L.; Noh, H.; Stone, A. D.; Cao, H. Time-Reversed Lasing and Interferometric Control of Absorption. *Science* **2011**, *331*, 889−892.
(29) Yin, H.; Dong, B.; Liu, X.; Zhan, T.; Shi, L.; Zi, J.; Yablonovitch, E. Amorphous diamond-structured photonic crystal in the feather barbs of the scarlet macaw. *Proc. Natl. Acad. Sci. U. S. A.* **2012**, *109*, 10798−10801.
(30) Helmrich, S.; Arias, A.; Lochead, G.; Wintermantel, T. M.; Buchhold, M.; Diehl, S.; Whitlock, S. Signatures of self-organized criticality in an ultracold atomic gas. *Nature* **2020**, *577*, 481−486.
(31) Shao, L.; Zhuo, X.; Wang, J. Advanced Plasmonic Materials for Dynamic Color Display. *Adv. Mater.* **2018**, *30*, 1704338.
(32) Kumar, K.; Duan, H.; Hegde, R. S.; Koh, S. C. W.; Wei, J. N.; Yang, J. K. W. Printing colour at the optical diffraction limit. *Nat. Nanotechnol.* **2012**, *7*, 557−561.
(33) Song, M.; Wang, D.; Peana, S.; Choudhury, S.; Nyga, P.; Kudyshev, Z. A.; Yu, H.; Boltasseva, A.; Shalaev, V. M.; Kildishev, A. V. Colors with plasmonic nanostructures: A full-spectrum review. *Applied Physics Reviews* **2019**, *6*, 041308.
(34) Daqiqeh Rezaei, S.; Dong, Z.; You En Chan, J.; Trisno, J.; Ng, R. J. H.; Ruan, Q.; Qiu, C.-W.; Mortensen, N. A.; Yang, J. K. Nanophotonic Structural Colors. *ACS Photonics* **2021**, *8*, 18−33.
(35) Franklin, D.; Chen, Y.; Vazquez-Guardado, A.; Modak, S.; Boroumand, J.; Xu, D.; Wu, S.-T.; Chanda, D. Polarization-independent actively tunable colour generation on imprinted plasmonic surfaces. *Nat. Commun.* **2015**, *6*, 7337.
(36) Li, J.; Yu, P.; Zhang, S.; Liu, N. Electrically-controlled digital metasurface device for light projection displays. *Nat. Commun.* **2020**, *11*, 3574.
(37) Chowdhury, S. N.; Nyga, P.; Kudyshev, Z. A.; Garcia Bravo, E.; Lagutchev, A. S.; Kildishev, A. V.; Shalaev, V. M.; Boltasseva, A. Lithography-Free Plasmonic Color Printing with Femtosecond Laser on Semicontinuous Silver Films. *ACS Photonics* **2021**, *8*, 521−530.
(38) Nyga, P.; Chowdhury, S. N.; Kudyshev, Z.; Thoreson, M. D.; Kildishev, A. V.; Shalaev, V. M.; Boltasseva, A. Laser-induced color printing on semicontinuous silver films: red, green and blue. *Opt. Mater. Express* **2019**, *9*, 1528−1538.
(39) Ouk Kim, S.; Solak, H. H.; Stoykovich, M. P.; Ferrier, N. J.; de Pablo, J. J.; Nealey, P. F. Epitaxial self-assembly of block copolymers on lithographically defined nanopatterned substrates. *Nature* **2003**, *424*, 411−414.
(40) Vynck, K.; Burresi, M.; Riboli, F.; Wiersma, D. S. Photon management in two-dimensional disordered media. *Nat. Mater.* **2012**, *11*, 1017−1022.
(41) Zheng, G.; Mühlenbernd, H.; Kenney, M.; Li, G.; Zentgraf, T.; Zhang, S. Metasurface holograms reaching 80% efficiency. *Nat. Nanotechnol.* **2015**, *10*, 308−312.
(42) Qin, F.; Ding, L.; Zhang, L.; Monticone, F.; Chum, C. C.; Deng, J.; Mei, S.; Li, Y.; Teng, J.; Hong, M.; Zhang, S.; Alú, A.; Qiu, C.-W. Hybrid bilayer plasmonic metasurface efficiently manipulates visible light. *Science Advances* **2016**, *2*, e1501168.
(43) Spägele, C.; Tamagnone, M.; Kazakov, D.; Ossiander, M.; Piccardo, M.; Capasso, F. Multifunctional wide-angle optics and lasing based on supercell metasurfaces. *Nat. Commun.* **2021**, *12*, 3787.
(44) Izumi, R.; Ikezawa, S.; Iwami, K. Metasurface holographic movie: a cinematographic approach. *Opt. Express* **2020**, *28*, 23761−23770.
(45) Joo, W.-J.; Kyoung, J.; Esfandyarpour, M.; Lee, S.-H.; Koo, H.; Song, S.; Kwon, Y.-N.; Song, S. H.; Bae, J. C.; Jo, A.; Kwon, M.-J.; Han, S. H.; Kim, S.-H.; Hwang, S.; Brongersma, M. L. Metasurface-driven OLED displays beyond 10,000 pixels per inch. *Science* **2020**, *370*, 459−463.


https://doi.org/10.1021/acs.nanolett.1c04874
Nano Lett. XXXX, XXX, XXX−XXX